MNRAS 000, 1–8 (2018) Preprint 17 December 2018 Compiled using MNRAS LATEX style file v3.0

The complex evolution of the X-ray binary transient MAXI J1807+132 along the decay of its discovery outburst

F. Jiménez-Ibarra,[1,2]★ T. Muñoz-Darias,[1,2] M. Armas Padilla,[1,2] D. M. Russell,[3] J. Casares,[1,2] M.A.P. Torres,[1,2] D. Mata Sánchez,[1,2,4,5] P. G. Jonker[4,6] and F. Lewis[7,8]

[1]*Instituto de Astrofísica de Canarias, Vía Láctea, La Laguna, E-38205, Santa Cruz de Tenerife, Spain*
[2]*Departamento de Astrofísica, Universidad de La Laguna, E-38206, Santa Cruz de Tenerife, Spain*
[3]*New York University Abu Dhabi, PO Box 129188, Abu Dhabi, UAE*
[4]*SRON, Netherlands Institute for Space Research, Sorbonnelaan 2, NL-3584CA Utrecht, The Netherlands*
[5]*Jodrell Bank Centre for Astrophysics, School of Physics and Astronomy, The University of Manchester, Manchester M13 9PL, UK*
[6]*Department of Astrophysics/IMAPP, Radboud University, P.O. Box 9010, NL-6500GL Nijmegen, The Netherlands*
[7]*Faulkes Telescope Project, School of Physics, and Astronomy, Cardiff University, The Parade, Cardiff, CF24 3AA, Wales, UK*
[8]*Astrophysics Research Institute, Liverpool John Moores University, 146 Brownlow Hill, Liverpool L3 5RF, UK*

Accepted XXX. Received YYY; in original form ZZZ

ABSTRACT

MAXI J1807+132 is an X-ray transient discovered during the decay of an outburst in 2017. We present optical and X-ray monitoring of the source over more than 125 days, from outburst to quiescence. The outburst decay is characterized by the presence of several re-flares with a quasi-periodic recurrence time of $\sim$ 6.5 days. We detect broad H and He emission lines during outburst, characteristic of transient low mass X-ray binaries. These emission lines show strong variability from epoch to epoch and, in particular, during the early stages are found embedded into deep and very broad absorption features. The quiescent spectrum shows Hα in emission and no obvious signatures of the donor star. *XMM-Newton* and *Swift* spectra can be fitted with standard X-ray models for accreting black-holes and neutron stars, although the obtained spectral parameters favour the latter scenario. Conversely, other observables such as the optical/X-ray flux ratio, the likely systemic velocity ($\gamma \sim -150$ km s^{-1}) and the re-flares recurrence time suggest a black hole nature. We discuss all the above possibilities with emphasis on the strong similarities of MAXI J1807+132 with short orbital period systems.

Key words: X-rays: binaries – stars: black holes – stars: neutron – accretion, accretion discs

1 INTRODUCTION

About a million X-ray sources have been detected after more than 50 years of X-ray astronomy. A fraction of these objects have been identified as low-mass X-ray binaries (LMXBs); binary systems harbouring a neutron star (NS) or a black hole (BH), which is accreting mass from a companion star typically less massive than the Sun. LMXBs provide a unique scenario to study extreme astrophysical phenomena such as accretion processes, the ejection of outflows and the final stages of the stellar evolution (e.g., Fender & Muñoz-Darias 2016; Casares & Jonker 2014). The subclass known as transient LMXBs spend most part of their lives in a dormant, quiescent state, but show brightening episodes (outbursts) when they increase their luminosity by several orders of magnitude (e.g., Remillard & McClintock 2006). A significant fraction of the X-ray photons are absorbed in the accretion disc and then re-emitted at lower energies. As a result, the optical spectra of LMXBs are typically flat and blue with strong superimposed emission lines of H, He I, and He II (e.g., Charles & Coe 2006).

X-ray and optical observations provide complementary information in the study of LMXBs. On one hand, the nature of the compact object and its properties can be constrained based on the presence of thermonuclear burst (Galloway et al. 2008), pulsations and other timing features (van der Klis 2006; Motta 2016), and the spectral/timing X-ray evolution (Belloni et al. 2011). On the other hand, dynamical solutions can be obtained from optical and near-infrared spectroscopy during quiescence (e.g., Casares et al. 1992). In addition, the inflow and outflow properties (e.g., winds) as well as some scale parameters are accessible when high-quality spectroscopy is achievable in the optical (e.g., Muñoz-Darias et al. 2016; Jiménez-Ibarra et al. 2018) or in X-rays (e.g., Miller et al. 2006; Díaz Trigo et al. 2006; Ponti et al. 2012).

MAXI J1807+132 is a new X-ray transient discovered on 13 March 2017 by the nova-search system of the Monitor of All-sky X-ray Image (MAXI, Negoro et al. 2017). The source is located 15 ° above the galactic plane at $\alpha, \delta = 18^{\rm h}08^{\rm m}07.549^{\rm s}, +13°15'05.40''$ (J2000, Kennea et al. 2017a,b). An optical counterpart consistent

★ E-mail: felipeji@iac.es

with the position of the transient was found in pre-outburst archival images of PanSTARRS-1 (Chambers et al. 2016).The object was identified in 31 multi-epoch images in 5 PanSTARRS-1 broadband filters: g, r, i, z, and y (Denisenko 2017). The average magnitude is $g \sim 21$ but shows variability of up to 1 magnitude from epoch to epoch ($\sigma \sim 0.8$ over 9 detections). Based on its high galactic latitude, soft X-ray spectrum, UV brightness, and a tentative association with a previous flaring event it was initially proposed as a candidate tidal disruption event (Negoro et al. 2017; Kennea et al. 2017c). However, the optical spectrum and other X-ray properties soon advocated for an X-ray binary association (Munoz-Darias et al. 2017; Shidatsu et al. 2017b; Armas Padilla et al. 2017b). Subsequently, Shidatsu et al. (2017a) favoured a NS accretor from analysis of *Swift* X-ray spectra in the range of 0.3 – 10 keV.

In this paper we present a detailed optical and X-ray study of MAXI J1807+132 during the decay of its 2017 outburst. We carried out a photometric follow-up in three SDSS bands (g, r, and i). Simultaneous optical spectroscopy was performed in 6 different epochs, both in outburst and quiescence. In addition, we analyse *XMM-Newton* archival observations taken soon after the MAXI alert.

2 OBSERVATIONS AND DATA REDUCTION

2.1 Optical data

The photometric observations were carried out from March 28 to July 12 of 2017 over 35 different epochs. The data were obtained in the SDSS-g,-r, and -i bands using the 2m Liverpool Telescope (LT) at the Observatorio del Roque de Los Muchachos (hereafter ORM) located in La Palma (Spain), and the 2-meter and 1-meter class telescopes from Las Cumbres Observatory (LCO). In addition, a continuous light-curve of 82 photometric points was taken (SDSS-r) using the 4.2-m William Herschel Telescope (WHT) at the ORM over a time-lapse of ~ 160 minutes on July 22. The WHT data were reduced using ASTROPY-CCDPROC based routines (Astropy Collaboration et al. 2013). Data from LCO were automatically processed through the BANZAI pipeline[1]. The LT data reduction was performed using the IO:O data reduction pipeline[2]. Flux calibration was carried out against nearby stars present in the PanSTARRs catalog.

We also obtained intermediate resolution spectroscopy using the Optical System for Imaging and low-Intermediate Resolution Integrated Spectroscopy (OSIRIS; Cepa et al. 2000) attached to 10.4m Gran Telescopio Canarias (GTC) at the ORM. We used the R1000B optical grism (2.12 Å pix^{-1} at 5455 Å) covering the spectral range 3630–7500 Å. This, in combination with a slit width of 1 arcsec, provided a spectral resolution of 360 km s^{-1} (measured as the full-width at half-maximum at ~ 5577 Å). A total of 5 spectra were obtained from March 28 to August 18. In addition, one spectrum was taken on July 2018 using the R1000R grism (2.62 Å pix^{-1} at 7430 Å) covering the range 5100–10000 Å. We reached a resolution of 381 km s^{-1} (full-width at half-maximum at ~ 5577 Å) using a slit width of 1 arcsec.

The spectroscopic data were de-biased and flat-fielded using IRAF standard routines. We used regular arc lamp exposures taken on each observing night to carry out the pixel-to-wavelength calibration (HgAr+Ne lamps for the R1000B grism and HgAr+Ne+Xe for the R1000R). Cosmic rays were removed from the data using L.A.Cosmic (van Dokkum 2001) before extracting the spectra. We used the O I 5577.338 Å sky emission line and the MOLLY software to measure and then correct the subpixel velocity drifts (< 100 km s^{-1}) introduced by instrumental flexure effects.

In addition, we used the acquisition images (SDSS-g and SDSS-r) to obtain photometric measurements contemporaneous with the spectroscopic observations (see Table 1). These were reduced in the same way as the WHT observations.

Table 1. Spectroscopy of MAXI J1807+132.

Spectrum	Date	Exp. time (s)	SDSS-g (mag)
1	28/03/2017	600 (2 × 300)	18.36 ± 0.01
2	30/03/2017	900 (2 × 450)	19.16 ± 0.03
3	06/04/2017	3600 (2 × 1800)	19.08 ± 0.02
4	16/07/2017	3000 (2 × 1500)	21.60 ± 0.23
5	18/08/2017	1003	21.51 ± 0.08
6	13/07/2018	1800	21.36 ± 0.01*

*SDSS-r

2.2 X-ray observations

2.2.1 *Swift data*

The Neil Gehrels *Swift* Observatory (Gehrels et al. 2004) pointed to MAXI J1807+132 on 29 occasions since it was reported as an active source. The on-board X-ray Telescope (XRT; Burrows et al. 2005) was operated in window timing (WT) mode for the first 4 pointings and in photon counting (PC) mode for the remaining observations. We used the `HEASoft` v.6.20 package to reduce the data. We processed the raw XRT data running the `xrtpipeline` task selecting the standard event grades of 0-12 and 0-2 for the PC and WT mode observations, respectively. With `Xselect` v2.4 we extracted the source events from a circular region of ~ 40 arcsec radius. To compute the background, we used three circular regions of similar size and shape on an empty sky region (PC observations), and an annulus centred on the source with an 195 arcsec inner radius and 275 arcsec outer radius for the WT data.

The source is detected in 16 out of the 29 observations (i.e., with signal-to-noise ratio > 3 σ), and only 4 of them have enough counts to carry out spectral analysis using χ^2 statistics (> 50 counts; see Fig. 1 top panel). For these observations, we created exposure maps and ancillary response files following the standard *Swift* analysis threads[3], and we acquired the last version of the response matrix files from the High Energy Astrophysics Science Archive Research Center (HEASARC) calibration database (CALDB). We grouped the spectra so as to attain a minimum of 10 photons per bin and, therefore, be able to use χ^2 statistics consistently.

2.2.2 *XMM-Newton data*

Two observations were acquired with the *XMM-Newton* observatory (Jansen et al. 2001) on March 29 and 30, 2017 (gap between them of less than 7 h), with exposures of 19 and 29 ksec, respectively. The configuration of the European Photon Imaging Camera (EPIC)

[1] Beautiful Algorithms to Normalize Zillions of Astronomical Images. Code available at https://github.com/LCOGT/banzai

[2] http://telescope.livjm.ac.uk/TelInst/Pipelines/#ioo

[3] `http://www.swift.ac.uk/analysis/xrt/`

was the same for both observations: MOS1 detector was operated in imaging small-window mode, and MOS2 and PN detectors in timing mode, all of them with the thin filter (Turner et al. 2001; Strüder et al. 2001). The source was not detected in the MOS2 camera. Due to strong episodes of background flaring, we proceeded to exclude data with count rates > 0.4 counts s^{-1} at energies >10 keV and > 0.5 counts s^{-1} at energies 10–20 keV for the MOS and PN cameras, respectively. For MOS1, we extracted source events from a circular region with a radius of 45 arcsec and a source-free circular region with a radius of 100 arcsec for the background. For PN, we extracted source and background events using the RAWX columns in [33:43] and in [10:18], respectively. Light curves and spectra, as well as associated response matrix files and ancillary response files were generated following the standard analysis threads[4]. For MOS1, we rebinned the spectrum in order to include a minimum of 25 counts in every spectral channel, avoiding to oversample the full width at half-maximum of the energy resolution by a factor larger than 3. In the case of PN, we rebinned the spectrum in order to have a minimum signal-to-noise ratio of 6.

3 RESULTS

3.1 Outburst evolution

Our photometric follow-up is presented in the middle panel of Fig. 1 and Table A1. It mostly includes photometric points in the SDSS-*g* band complemented with measurements in SDSS-*r* and -*i*. The photometric monitoring started while the source was decaying from the outburst peak. Our first data point is almost 3 mag brighter than the quiescence magnitude reported by Denisenko (2017). Over the next 9 days the source gradually decayed from $g \sim 18.8$ to quiescence ($g \sim 21$). Subsequently, we observed an abrupt rise of ~ 2.7 mag in two days. We identify up to 7 re-brightening events superposed on a decay profile during the ~ 70 days following the main outburst. This activity is detected in all the photometric bands studied. The secondary peaks have amplitudes of ~ 2 mag above the quiescent level. A tentative periodic recurrence of ~ 6 days is observed in the brightest 4 events (see Section 4.1).

During the photometric monitoring, 6 optical spectra were obtained (and labelled chronologically spectrum-1 to -6 hereafter). These are presented in Fig. 2. The first 3 spectra were taken when the source was brighter than $g \sim 19.5$, while the remaining found the source in quiescence at $g \sim 21$ (see Fig. 1 and Table 1). Hereafter, we refer to them as bright and faint spectra, respectively. The source showed pronounced spectral variability as it evolves through its complex outburst decay. We observed several emission lines in the bright spectra that are commonly seen in LMXBs in outburst. For example, spectrum-1 exhibits the Balmer series up to Hγ as well as He II 4686 Å. Less evident He I lines at ~ 5875 Å and ~ 6679 Å can be also identified. Fainter Balmer lines are present in the remaining bright spectra. Conversely, we can not distinguish He transitions in spectrum-2 and -3. In addition, the Balmer emission lines appear embedded in broad absorptions that are stronger for the bluest lines. This pattern is particularly noticeable in spectrum-3, but it is still recognizable in spectrum-1 and -2. We note that spectrum-2 and -3 were obtained at comparable magnitudes (19.22 ± 0.02 and 19.06 ± 0.02 SDSS-*g* mag, respectively) but they show significant differences. Spectrum-2 is morphologically closer to spectrum-1. However, for spectrum-3 the broad absorptions are remarkably deep and dominate over the emission lines.

We also observed morphological differences between faint spectra. Spectrum-4 and -5 are featureless while spectrum-6 only exhibits Hα in emission. Absorption lines that could be associated with the companion star are not detected in any of the spectra.

3.2 Emission lines properties

We measured Doppler shifts in the emission lines observed in the spectrum-1,-2, -3, and -6 by fitting a multi-Gaussian model to previously normalised spectra. The lines considered and the model applied to each spectrum varies slightly from one to another following the morphological differences between them. For instance we modelled the Balmer lines and He II emission line in spectrum-1, while only Hα was fitted in spectrum-6. In order to obtain more reliable velocity measurements the separations between Gaussians were fixed. The broad absorptions underneath were taken into account when modelling the Balmer lines in spectrum-1,-2, and -3. To this end, we fitted broad Gaussian profiles keeping the relative separations between them fixed as in the case of the emission lines. We used a 2-Gaussian model to account for the broad absorption components in the line profiles when present. The broadening effect on the emission lines due to the instrumental resolution was taken into account in the modelling. The results are shown in Fig. 3.

The derived emission line centroid velocities are presented in Table 3. In spectrum-3 the velocity obtained relies only on 2 emission lines strongly affected by the absorptions, and thus the uncertainty on the centroid velocity is a factor of ~ 2 larger than that from spectrum-1. The derived velocities are consistent with each other within 1.5 σ. We can tentatively associate these velocity shifts with the velocity of the centre of mass of the system, projected along the line of sight, γ. We note that, on one hand, it seems unlikely that the 3 outburst spectra were taken at the same orbital phase and reflect the projected velocity of a particular structure of the accretion disc. On the other hand, it is highly unlikely that these velocities arise from some region (or regions) in the system showing the same radial velocity at different orbital phases. This argument is strongly favoured by the velocity measured from spectrum-6, taken more than a year later. We propose the average value $\gamma = -145 \pm 13$ km s^{-1} as the systemic velocity of the binary, although a radial velocity curve is required to obtain a conclusive result.

The offset measured in the absorption components observed in spectrum-1, -2, and -3 are centred at ~ 80 km s^{-1} showing uncertainties bigger than ~ 190 km s^{-1}. Hence, we cannot constrain the velocity from these offsets.

We determined the FWHM of the emission lines from the multi-Gaussian fitting described above. In addition, we individually fitted the Hα emission line and its broad absorption profile with a double Gaussian model in spectrum-1,-2, and -3. Table 3 shows both the FWHM from all the emission lines considered and that from Hα for each spectra. The measured FWHM of the broad components are 2851 ± 223, 4260 ± 531, and 2303 ± 45 km s^{-1} for spectrum-1,-2, and 3, respectively. Finally, the equivalent width (EW) of the Hα emission line in the spectra which are not contaminated by the absorption component are 1.96 ± 0.11 Å (spectrum-1), 2.89 ± 0.20 Å (spectrum-2) and 6.86 ± 0.70 Å (spectrum-6), whilst He II has EW 1.35 ± 0.17 Å in spectrum-1.

[4] https://www.cosmos.esa.int/web/xmm-newton/sas-threads

Table 2. Results from the X-ray spectral fits.

Instrument/ Obs ID	$kT_{\rm bb/in}$ (keV)	$N_{\rm bb/in}$	Γ	$F_{\rm X,unabs}$ (10^{-12} erg cm^{-2} s^{-1})	$T_{\rm fr}$ (%)	χ^2_ν (dof)
Swift/XRT			TBABS*(POWERLAW)			
00010037001	–	–	2.01 ± 0.06	19.1 ± 1.5	–	1.37 (145)
00010037002	–	–	2.1 ± 0.1	5.6 ± 1.0	–	0.89 (59)
00010037004	–	–	2.6 ± 0.8	0.33 ± 0.1	–	0.62 (25)
00010037017	–	–	1.8 ± 0.2	5.7 ± 1.4	–	1.06 (22)
XMM/EPIC			TBABS*(BBODYRAD+NTHCOMP(BB))			
	0.21 ± 0.01	111 ± 10	2.1 ± 0.1	6.42 ± 0.1	25	1.01 (576)
			TBABS*(DISKBB+NTHCOMP(DISK))			
	0.33 ± 0.01	15 ± 2	1.8 ± 0.1	6.7 ± 0.1	36	0.96 (576)

Note. – Quoted errors represent 90% confidence levels. $F_{\rm X,unabs}$ represent the unabsorbed fluxes in the 2–10 keV and 0.5–10 keV bands for *Swift* and *XMM-Newton* observations, respectively. $T_{\rm fr}$ reflects the fractional contribution of the thermal component to the total unabsorbed 0.5–10 keV flux. When using NTHCOMP we coupled $kT_{\rm seed}$ to the temperature of the thermal component (i.e., $kT_{\rm disc}$ or $kT_{\rm bb}$; see Section 3.4.2)

Table 3. Parameters from the observed emission lines. FWHM refers to the ensemble of all the emission lines

Spectrum	FWHM (km s^{-1})	Centroid velocity (km s^{-1})	Hα FWHM (km s^{-1})
1	796 ± 57	-106 ± 17	750 ± 63
2	557 ± 64	-147 ± 21	630 ± 74
3	468 ± 106	-169 ± 31	499 ± 142
6	–	-157 ± 35	698 ± 89

3.3 Extinction along the line of sight

The depth of interstellar absorption bands can be used to estimate the extinction along the line of sight. In particular, the color excess E_{B-V} is correlated with the EW of the strongest component of the Na I doublet (NaD1, 5890 Å). This correlation is valid for EWs $\lesssim 0.5$ Å (Munari & Zwitter 1997). In the bright spectra we observed the two components of the Na I doublet blended in a single absorption feature. No Na I components were detected in the faint spectra, which are contaminated by nearby sky emission lines (see Fig. 2). We averaged the 3 bright spectra and derived EW = -1.10 ± 0.08 Å. This implies that the line is saturated and only a lower limit $E_{B-V} \geq 0.3$ can be derived. This corresponds to $N_H \gtrapprox 2.4 \times 10^{21}$ cm^{-2} when applying the dust to gas relation ($N_H = 2.87 \times 10^{21}$ cm^{-2} A_V; Foight et al. 2016) converting using the canonical relation $A_V = 3E_{B-V}$. This value is still roughly consistent with the Galactic value, $N_H \sim 1 \times 10^{21}$ cm^{-2} (Kalberla et al. 2005).

3.4 X-ray analysis

We used XSPEC (v.12.9.1; Arnaud 1996) to analyse the X-ray spectra. In order to account for interstellar absorption, we used the Tuebingen-Boulder Interstellar Medium absorption model (TBABS in XSPEC) with cross-sections of Verner et al. (1996) and abundances of Wilms et al. (2000). We assumed a constant hydrogen equivalent column density of $N_H = 1 \times 10^{21}$ cm^{-2} consistent with the low reddening expected for this direction (see previous section) and Shidatsu et al. (2017a).

3.4.1 *Swift*

We used a simple power-law model to fit the 4 *Swift* spectra. We calculated the 2–10 keV unabsorbed flux in order to plot these points in the Optical/X-ray correlation (see Section 3.5). We refer the reader to Shidatsu et al. (2017a) for more details on the *Swift* observations.

3.4.2 *XMM-Newton*

We simultaneously fit the 0.5-10 keV MOS1 and 0.7-10 keV PN spectra by using tied spectral parameters of both *XMM-Newton* observations. We included a constant factor (CONSTANT) fixed to 1 for PN spectra and free to vary for MOS1 spectra so to account for cross-calibration uncertainties between the instruments.

We used a simple 2-component model to fit the spectra. We combined a soft component to account for either emission from an accretion disc or from a possible NS surface/boundary-layer, and a hard component to model the inverse-Compton emission from the Corona. Thus, we used a multicolour disc or single black body (BB) plus a thermally Comptonized continuum model (i.e., DISKBB+NTHCOMP and BBODYRAD+NTHCOMP in XSPEC; Mitsuda et al. 1984; Makishima et al. 1986; Zdziarski et al. 1996; Życki et al. 1999). We assumed that the up-scattered photons arise from the associated thermal component. Thus, we coupled $kT_{\rm seed}$ to either $kT_{\rm disc}$ or $kT_{\rm bb}$, respectively, and changed the seed photons shape parameter accordingly (*im-type* in NTHCOMP). The two spectral models return acceptable fits ($\chi^2 \sim 544$-584 for 576 dof). The former yields a Comptonization asymptotic power-law photon index (Γ) of 1.8 ± 0.1 and a disc temperature of $kT_{\rm diskbb} = 0.33 \pm 0.01$ keV with a $N_{\rm in} = 15 \pm 2$. The latter translates to an unrealistic small internal disc radius ($R_{\rm in} \sim 5$ km applying the correction of Kubota et al. 1998; see also Armas Padilla et al. 2017a, and references therein) and compact object mass for a BH case (e.g., Tomsick et al. 2009). However, we note that it is not straightforward to obtain physically meaningful $R_{\rm in}$ values from this kind of modelling. We further discuss this in section 4.2. The inferred 0.5–10 keV unabsorbed flux is $(6.7 \pm 0.1) \times 10^{-12}$ erg cm^{-2} s^{-1}, from which ~ 36 per cent is produced by the thermal component. On the other hand, by using BBODYRAD+NTHCOMP we obtained $kT_{\rm bb} = 0.21 \pm 0.01$ keV and $N_{\rm bb} = 111 \pm 10$ while Γ is 2.1 ± 0.1. The inferred 0.5–10 keV unabsorbed flux is $(6.4 \pm 0.2) \times 10^{-12}$ erg cm^{-2} s^{-1}, from which $\sim$

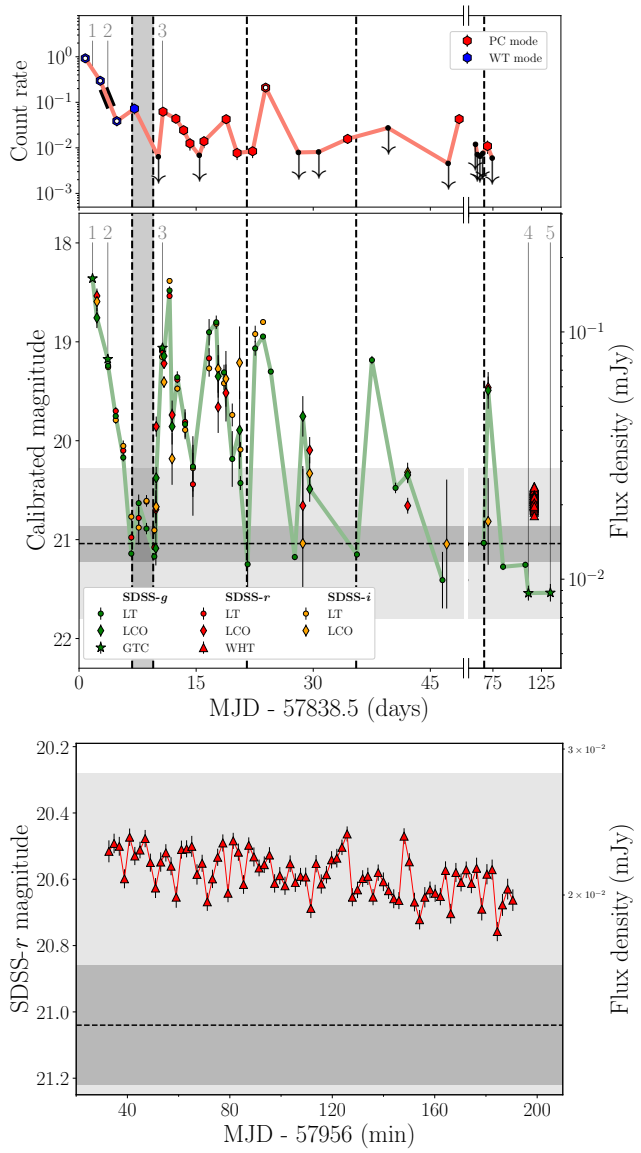

Figure 1. Top panel: X-ray light curve obtained with *Swift*/XRT. The thick black line indicates the *XMM-Newton* epochs. The observations employed in the spectral analysis are indicated as open symbols. Middle panel: Photometric follow-up of MAXI J1807+132 in the SDSS-*g*, -*r*, and -*i* bands (green, red and yellow markers, respectively). LT data are indicated by dots, while LCO data are marked as diamonds. At the end of the series, triangles show WHT points. GTC photometry from acquisition images is represented as stars and labelled in correspondence with spectra, except for the SDSS-*r* point and its corresponding spectrum taken on July 2018 ; Table 1. The light green, solid line joins the *g*-band points chronologically. The black dashed line shows the quiescence PanSTARRS *g*-band magnitude (after stacking) with its corresponding error displayed as dark grey area (21.04 ± 0.18; Denisenko 2017). The standard deviation of the 9 pre-outburst epochs is indicated as a light grey area. The vertical dashed lines (and grey band) indicate epochs consistent with optical quiescence where the source is detected in X-rays. Bottom panel: Zoom in of the WHT light-curve spanning 160 min.

25 per cent is produced by the thermal component. It is important to bear in mind that due to the lack of data above 10 keV and the low statistics, we were not able to constrain the temperature of the electron corona (kT_e), that was fixed to either 20 keV or 100 keV, typical values for NSs and BHs in the hard state (Burke et al. 2017). This value do not have an impact on the obtained results (within errors). The best fit results are reported in Table 2 and Fig. 4 with uncertainties given at 90 per cent confidence level.

As described above, the 2-component approach provides a good description of the data. However, we also tried other solutions. For instance, a simpler one-component model using a NTHCOMP was tested considering both scenarios: seed photons arising from a blackbody or from a disc blackbody. As expected, this forced the photon index to adopt higher values ($\Gamma = 2.48 \pm 0.03$) leaving significant residuals at high energies (χ^2 of 652 and 665 for 577 dof, respectively). This is reflected in the F-test, which yields a probability lower than 10^{-15} of improving the fit by chance when including a thermal component. In addition, more complex X-ray fitting, such as that provided by the three-component model proposed for NSs (e.g., Lin et al. 2007; Armas Padilla et al. 2017a) was also considered. However, even if this also reproduces the data, it does not produces a significant improvement and its use is not justified given the limited quality of the data and the relatively narrow spectral coverage of *XMM-Newton*.

3.5 Optical/X-ray correlation

Based on quasi-simultaneous optical/near-infrarred and X-ray observations of a large number of BHs and NSs, Russell et al. (2006) presented an empirical correlation between the nature of the compact object and its optical to X-ray luminosity ratio.

Fig. 5 shows the optical-X-ray luminosity diagram plotted using data from Russell et al. (2006, 2007). We investigate the location of MAXI J1807+132 on this diagram in order to constrain the nature of the compact object. To this end, we use 5 luminosity ratios, obtained from a quasi-simultaneous optical and X-ray data. To compute the luminosities, we consider 3 possibles distances: 1, 5, and 25 kpc. The optical/X-ray luminosity ratio suggests a BH nature for distances $\gtrsim$ 5 kpc. For closer distances the source sits on a transitional and poorly sampled region in between the BH and NS populations. A NS accretor is favoured if the distance is $\sim$ 1 kpc or lower.

3.6 Quiescence photometry

The bottom panel of Fig. 1 shows the SDSS-*r* light curve of MAXIJ1807+132 obtained on July 22, 2017 using the WHT. The source showed a mean brightness of 20.584 ± 0.003 mag, that is, $\sim$ 0.6 mag above the quiescence level reporter by Denisenko (2017). The light curve shows a complex behaviour dominated by flickering with an amplitude of up to $\sim$ 0.3 mag and a variance of 0.06 mag with respect to the mean (this correspond to 0.0013 mJy over a mean of 0.021 mJy). We explored the WHT dataset seeking for periodic oscillations using standard Lomb-Scargle techniques, but no modulations were found within the $\sim$ 2.5 hours observed.

4 DISCUSSION

We presented a detailed optical and X-ray follow up of MAXI J1807+132 during its 2017 outburst decay. This includes optical spectroscopy using GTC-10.4m, which reveals emission

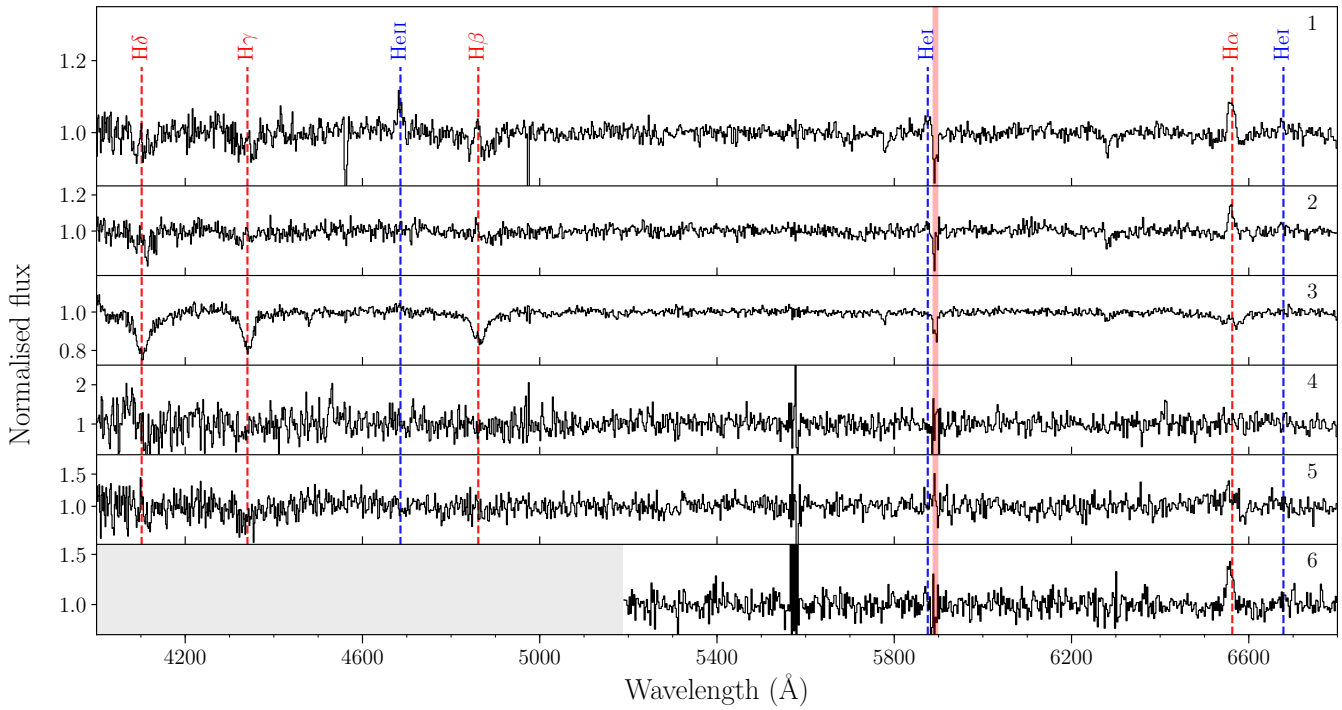

Figure 2. Multi-epoch spectroscopy of MAXI J1807+132 from GTC-OSIRIS (R1000B grism spectrum-1 to -5 and R1000R spectrum-6). Hydrogen (red) and He (blue) transitions are indicated by dashed lines. The Na I doublet is indicated as a red shadowed area at 5892 Å. Spectrum-4, -5 , and -6 show strong residuals caused by sky subtraction at ~ 5577 and ~ 5890 Å.

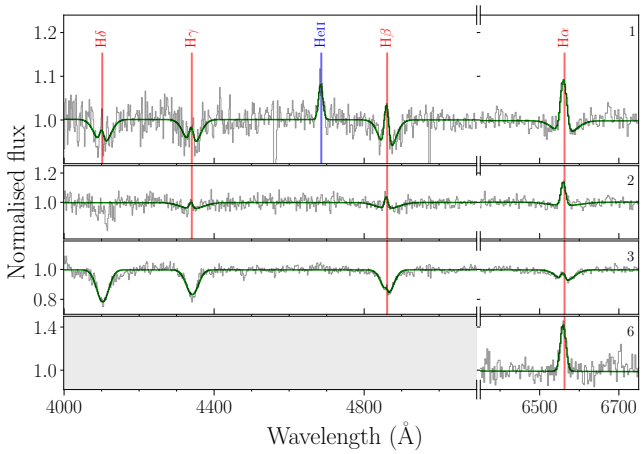

Figure 3. Trimmed spectra showing identified emission lines. The vertical lines represent the rest frame position of the transition used on each model (red for the Balmer series and blue for He II 4686 Å). Green line shows the resulting model.

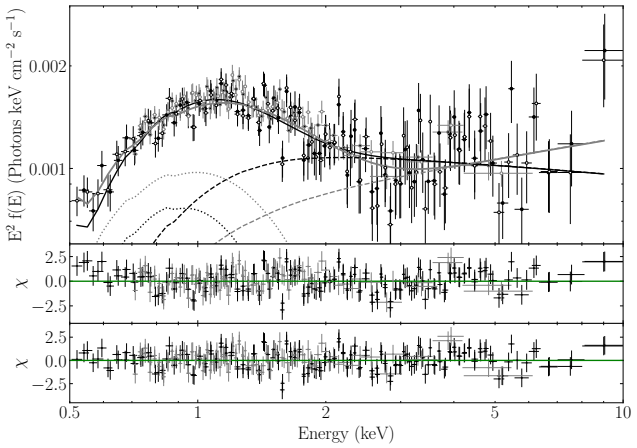

Figure 4. Top panel: Unfolded MOS1 (black) and PN (grey) spectra of the March 29 (filled symbol) and 30 (open symbol) *XMM-Newton* observations. The solid black line represents the best fit for the BBODYRAD+NTHCOMP model, the thermal component is shown as a dotted line and the Comptonized component as a dashed line. In grey is represented the same for the DISKBB+NTHCOMP model. Middle panel: Residuals in units of σ when using BBODYRAD+NTHCOMP model. Botton panel: Residuals in units of σ when using DISKBB+NTHCOMP model.

lines typically observed in LMXB spectra. The Balmer series appears in emission superposed to broad absorption features that are deeper towards the blue. Similar line profiles were observed before in other LMXBs (e.g., Nova Velorum 1993, GRO J0422+32, XTE J1118+480, XTE J1859+226; Bailyn & Orosz 1995; Casares et al. 1995; Dubus et al. 2001; Zurita et al. 2002, respectively). This can be interpreted as the result of emission lines being originated from photoionization in an optically thin region above the disc, combined with absorption lines arising from inner optically thick regions. The absorption throats were discussed in detail by Dubus et al. (2001). They found that the formation of these features is favoured by (hard X-ray) irradiation, since hard X-ray photons can

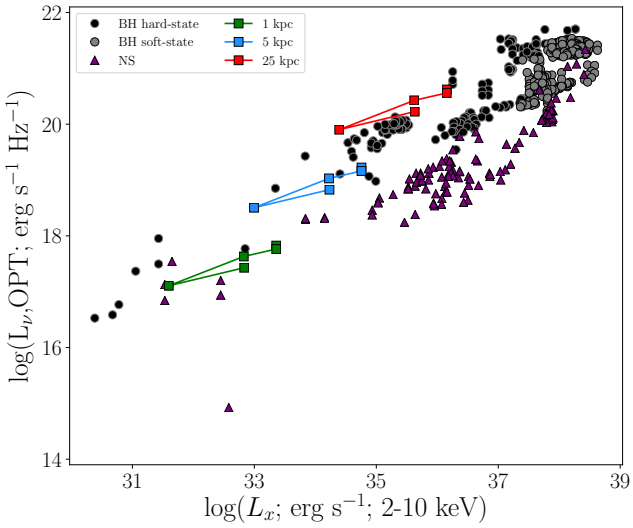

Figure 5. Optical-X-ray luminosity diagram (data from Russell et al. 2006, 2007). BHs in the hard and soft states are indicated as black and grey circles, respectively; NSs are plotted as violet triangles. Our data for MAXIJ1807+132 are overplotted assuming 3 distances: 1 kpc (green square), 5 kpc (blue square), and 25 kpc (red square).

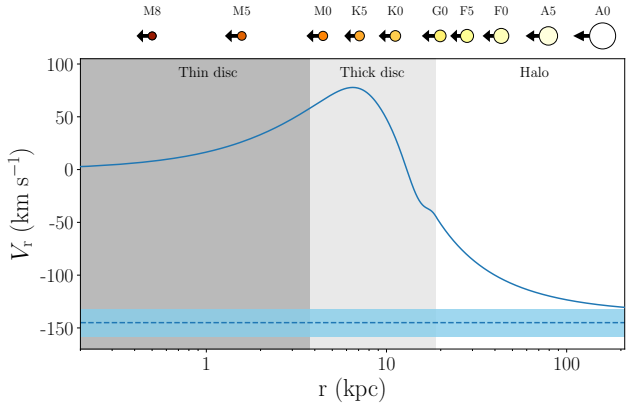

Figure 6. Radial velocity in the direction of MAXI J1807+132 as a function of r from the rotation curve of the Galaxy of Clemens (1985, blue solid line). Shadowed areas indicate the extension of the thin disc ($0 \leq z < 1$ kpc), the thick disc ($1 \leq z \leq 5$ kpc), and the halo ($h > 5$ kp) projected on r (Gilmore1983). The systemic velocity proposed and its corresponding error ($\gamma = -145 \pm 13$ km s^{-1}) are indicated as a blue dashed line. Top axis shows the spectral type of a main sequence star of $g \sim 21$ placed at a distance r.

access deeper disc. In addition, these features are not expected in high inclination systems, since the absorptions tend to disappear as the inclination increases, affected by the limb darkening in the two-dimensional disc picture. If this interpretation is correct, it would suggest an intermediate to low orbital inclination for the system. However, we note that both GRO J0422+32 and XTE J1118+480 have intermediate to high inclinations (45° ± 2 and 68–79°; Gelino & Harrison 2003; Khargharia et al. 2012), respectively.

We have measured a systematic velocity offset in the emission lines observed both in outburst and quiescence, that we interpret as the binary systemic velocity ($\gamma = -145 \pm 13$ km s^{-1}). We now consider a simple kinematic model for the Milky Way to compare the observed γ with the radial velocity expected for a given distance in the direction of the source [i.e., $V_r(r, l, b)$ where r is the heliocentric distance]. We use the rotation curve from Clemens (1985), which is defined both in the inner and outer Galaxy, and assumes that the Milky Way follows a pure circular motion. Fig. 6, shows the radial velocity in the direction $(l, b) = (40°.12, 15°.50)$ as a function of r. The kinetic model predicts negative radial velocities beyond $r \sim 10$ kpc, while velocities consistent with the measured γ are only expected for $r > 100$ kpc. Clearly the observed systemic velocity cannot be explained by the rotation curve of the Galaxy, not even if the object is located in the very outskirts of the Galaxy. We also use b to determine the vertical distance above the Galactic plane (z) as a function of r. Shadowed areas on Fig. 6 indicate the extension of the thin disc ($0 \leq z < 1$ kpc), the thick disc ($1 \leq z \leq 5$ kpc), and the halo ($z > 5$ kpc) projected on r (Gilmore & Reid 1983). We observe that the Galactic rotation could account for the measured radial velocity only if the source is located in the outer halo. For lower elevations the source requires a significant peculiar velocity, whether it belongs to the thin disc or to the thick disc. Such high peculiar velocities have been observed in LMXBs and are typically interpreted as natal kicks resulted from asymmetries in the supernova explosion.

Finally, assuming that the quiescent light is dominated by the companion star, it is possible to estimate its spectral classification based on the quiescent magnitude (Denisenko 2017). However, the high variability observed suggests that the disc emission is significant even in quiescence. We therefore infer an upper limit to the expected spectral type of the donor for the case of a main sequence star at a given distance (assuming $g \sim 21$). The results are schematically presented in the top axis of the Fig. 6

4.1 Reflares during the decay

We detected up to 7 brightening episodes during the outburst decay. A quasi-periodic recurrence can be noticed by visual inspection (Fig. 7). We computed a Lomb-Scargle periodogram of the SDSS- g points between MJD 57848–57885, when the brightening episodes are observed and resolved (i.e., sampling better than one point every 3 days). The light curve analysed and the resulting periodogram are shown in Fig. 7. The periodogram was produced using the LombScargle-python class (VanderPlas 2017). We find the highest power at ~ 0.15 d^{-1} that yields a period of 6.5 days. The origin of these periodic brightening episodes is uncertain, but it has been proposed they might be related to a cyclical mechanism involving the accretion rate (Chen et al. 1993; Augusteijn et al. 1993; Mineshige 1994). In the context of the model proposed by Augusteijn et al. (1993) the brightening episodes or reflares are "echoes" of the main outburst. X-ray illumination of the companion star triggers enhanced mass transfer and subsequent mini-outbusts. Within this picture, the recurrence time of each re-brightening is the time that a perturbation takes to travel across the accretion disc radius ($R_{\rm out}$). The heating front propagates at $v \approx \alpha v_{\rm s}$, where α is the viscosity parameter and $v_{\rm s}$ the sound speed (Lasota 2001). Under the assumption of a hot accretion disc ($\alpha = 0.1$ and $v_{\rm s} = 15$ km s^{-1}, Menou et al. 1999), we obtain $R_{\rm out} \sim 8.4 \times 10^{10}$ cm. Using this $R_{\rm out}$ we estimate the binary period (P) using $R_{\rm out} \simeq 1.2 \times 10^{11} M^{1/3} P^{2/3}$ [cm], where M is the mass of the compact object expressed in $M_\odot$ (King et al. 1996). We adopt the two canonical masses for compact stars, 1.4 $M_\odot$ for a NS and 8 $M_\odot$ for a BH. We obtained P(NS) $\sim$ 12 h and P(BH) $\sim$ 5 h, respectively.

Using the above orbital periods, we can calculate the mean

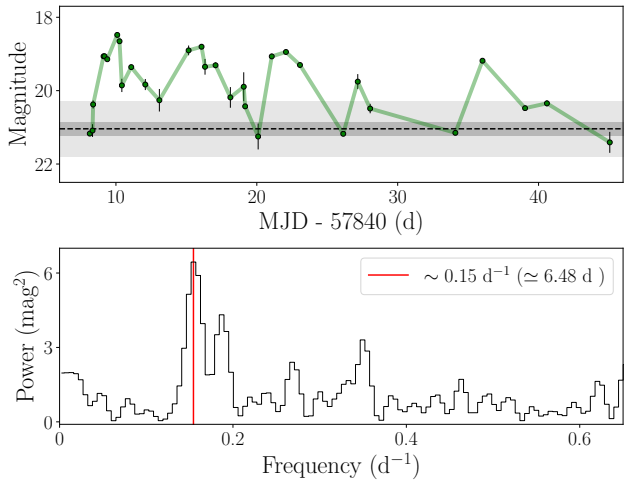

Figure 7. Top panel: Segment of the SDSS-*g* light curve used for the Lomb-Scargle analysis. Bottom panel: Resulted Lomb-Scargle periodogram from the data in the top panel. The red line indicates the position of the strongest peak that corresponds to ~ 0.15 d^{-1} ($\simeq 6.56$ d).

density of the companion star that fills its Roche lobe (Faulkner et al. 1972), and compare it with that of typical main sequence stars (Cox 2000). We find that, for the case of a BH, the donor would be a M0–M2 main sequence while for the case of a NS it would be a F0–F5 main sequence. The distance to the system can be inferred in both cases, if we combine the lower limit to the quiescent magnitude and the spectral types above. The source is expected to be at $\gtrsim 4$ kpc and $\gtrsim 35$ kpc for a BH and NS system, respectively (see Fig. 6). We note that only the BH case is consistent with the constraints devised by the optical/X-ray luminosity diagram. All in all, these broad observational properties seem to support the case of a BH binary instead of a NS.

For simplicity, we have considered in the above a main sequence companion star. However, we note that a somewhat evolved donor cannot be ruled out. Indeed, subgiant companions are thought to be present in some LMXBs with orbital periods $\gtrapprox 2$ d (e.g., V404 Cygni, GX 339-4 and XTE J1550-564; King 1993; Muñoz-Darias et al. 2008, respectively). For instance, in the case of GX 339-4, the 'stripped-giant' model predicts magnitudes in the range of $r \sim 21$–24 for a distance within ~ 6–15 kpc. This magnitude range is compatible to that observed in MAXI 1807+132 during quiescence (PanSTARRS-1 broadband filters $r = 21.19 \pm 0.09$ Denisenko 2017). We also explored the possibility of a giant (luminosity class III) companion star. We assumed the observed quiescent magnitude to be the magnitude of the donor, and compared it with that expected for a field giant at given distance. Using the absolute magnitudes tabulated in Cox (2000) we obtained a distance in the range of ~ 100–180 kpc, which effectively discards a giant companion.

4.2 On the nature of the compact object

The definitive determination of the nature of the compact object in an LMXB requires of either the detection of unequivocal NS features (i.e., pulsations or thermonuclear burst) or, alternatively, a dynamical measurement of the mass of the compact object. When none of the above is available, the likely nature of the accretor can be studied based on other observables:

- X-ray spectral properties. Albeit both NS and BH transients share a common phenomenology during outburst (e.g., Muñoz-Darias et al. 2011; Muñoz-Darias et al. 2014), the X-ray spectral modelling usually requires of an extra component to account for the emission from the NS surface (or its surroundings; e.g., Lin et al. 2007; Armas Padilla et al. 2017a, 2018). Using this argument Shidatsu et al. (2017a) favoured a NS nature based on spectral fitting of the *Swift* data. Here, we have also included deeper *XMM-Newton* observations in the X-ray spectral analysis. Although we are able to fit our data with both BH-like and NS-like spectral models, some of the spectral parameters are more similar to those typically obtained for NS systems at low accretion regimes. In particular, the low disc normalization ($N_{\rm in} = 15$) and the $\sim 30\%$ thermal contribution to the total flux (0.5–10 keV) challenge the BH scenario. BH systems at low luminosities reveal cold disc components, but these tend to have much larger normalization values (a proxy for the inner disc radius) and provide in most of the cases lower contributions to the observed flux (e.g., Reis et al. 2010; Armas Padilla et al. 2014a; Shidatsu et al. 2014; Plant et al. 2015). On the other hand, several NS LMXBs accreting at low luminosities show thermal fractions consistent with those reported in this work. These have been observed in both persistent (e.g., Armas Padilla et al. 2013; Degenaar et al. 2017; Armas Padilla et al. 2018) and transient systems (e.g., Degenaar et al. 2013; Campana et al. 2014; Arnason et al. 2015). In addition, we can compare the $\Gamma = 2.48 \pm 0.03$ obtained when solely using the Comptonization component with the photon index/X-ray luminosity diagram presented in Wijnands et al. (2015), which shows a distinctive evolution for BHs and NSs at $L_{\rm X} < 10^{36}$ erg s^{-1}. Even if the distance to MAXI J1807+132 (and therefore the luminosity) is not constrained, we find that a NS accretor is qualitatively favoured. All in all, our X-ray fitting agree to some extent with Shidatsu et al. (2017a) and favours a NS nature. However, it is important to bear in mind that a BH-like spectral modelling provides an equally good fit to the data, with the exception of the low normalization value of the disc component. Nevertheless, we note that we are using data with limited signal-to-noise and simple (Newtonian) disc models. Thus, we conclude that only from the X-ray fitting point of view we are not able to definitely constrain the nature of the compact object.

- The optical/X-ray luminosity diagram. This tool was initially presented by Russell et al. (2006) and has been subsequently applied to several objects (e.g., Armas Padilla et al. 2011; Hernández Santisteban et al. 2018). This test produces a "qualitative" classification, and strongly relies on the distance to the source. In Fig. 5 we show that a BH nature is clearly favoured for $d \gtrsim 5$ kpc, while lower distances would also allow for a NS accretor. This latter case is significantly favoured for very low distances ($d \lesssim 1$ kpc).

- We have estimated the systemic velocity from the optical spectra (Sec. 3.2). We find that it is likely large and negative ($\gamma \sim -150$ km s^{-1}). Comparing this value with the rotation curve of the Galaxy (Fig. 6) it is clear that a natal kick would be needed to explain γ, unless the system is located unrealistically far away. In addition, distances between ~ 5 and 10 kpc would require very high proper motions in excess of ~ 200 km s^{-1}. In any case, for $d \gtrsim 5$ kpc (i.e., BH scenario according to the optical/X-ray ratio) the system would be located in the thick disc, which itself favours a natal kick to explain such a large height above the Galactic plane (Repetto et al. 2012). We note that a population of transient BH-LMXBs is known to be present at these high latitudes (see e.g., Mata Sánchez et al. 2015; Kuulkers et al. 2013, and references therein). Interestingly, several of these BH systems have relatively short orbital periods (see table 2 in Shahbaz et al. 2013). On the other hand, at very close distances, systemic velocities within the range observed

in NS-LMXBs would be required (Ramachandran & Bhattacharya 1997; Mata Sánchez et al. 2015). Both, a large height above the Galactic plane and a close distance agree with the low extinction along the line-of-sight detected in X-rays (Sect. 3.3).

• Orbital period estimates from re-flares. The presence of several optical re-flares is one of the most relevant characteristics of the outburst decay of MAXI J1807+132. This kind of phenomena has been observed previously in cataclysmic variables (e.g., Patterson et al. 1998) but also in several BH transients such as XTE J1118+480, XTE J1859+226, and GRO J0422+32 (see Zurita et al. 2006, and references therein) and NSs systems (e.g., Torres et al. 2008; Patruno et al. 2016). These binaries have orbital periods of 4.1, 6.6, and 5.1 hr, respectively (Corral-Santana et al. 2016). For the case of GRO J0422+32 the re-flare recurrence time can be estimated and it is about 7-8 days (see e.g. fig. 2 in Zurita et al. 2006). This is remarkably similar to the one we have measured in MAXI J1807+132 (6.5 days) and from which we have inferred an orbital period of $\sim$ 5 h should the compact object be a BH (Sec. 4.1). Therefore, it seems that the proposed scenario (irradiation induced changes in mass transfer) might work for GRO J0422+32 and for extension for MAXI J1807+132. If this is the case, the NS scenario is clearly disfavoured, as it would imply an orbital period of $\sim$ 12 hours, which would place the source at $\gtrsim$ 35 kpc (see above). At this large distance the optical luminosity diagram strongly suggests a BH nature.

• X-ray detections near optical quiescence. Finally, it is worth mentioning that MAXI J1807+132 is detected in X-rays at optical magnitudes consistent with optical quiescence (e.g., grey band in Fig. 1). This naively suggest that (i) the system might be also close to X-ray quiescence and (ii) it might be relatively nearby as truly quiescent LMXBs can be only detected within a few kpc and using deep *XMM*/*Chandra* observations (e.g., Armas Padilla et al. 2014b, and references therein). By stacking several *Swift* observations around day 75 (see Fig. 1) and assuming a power-law spectrum with a photon-index of 2 with $N_{\rm H} = 1 \times 10^{-21}$ cm^{-2} we obtain an unabsorbed flux of 2.8×10^{-13} ergs s^{-1}. The combined count-rate is slightly lower than our faintest detection, so this stacking is effectively our dimmest detection of the source. By Imposing the lowest X-ray quiescence luminosities observed in LMXBs, that is, 0.5×10^{31} (BH) and 5×10^{31} (NS) ergs s^{-1} (fig. 3 in Armas Padilla et al. 2014b), we place lower limits to the distance of 0.5 and 1.5 kpc for a BH and a NS, respectively. These values would imply very late spectral type donors, even within the brown dwarf regime (Fig. 6). However, it seems more likely that the source is not in X-ray quiescence between re-flares as it usually takes several months to reach this state. In addition, the "optical quiescence" detected by PanSTARRs and in this work could be far from true optical quiescence. This is supported by the apparent lack of companion star features in the faintest spectra and by the flickering observed in the WHT lightcurve (Fig. 1). We note that even if our faintest detection (see above) corresponds to luminosities as low as 1×10^{33} ergs s^{-1} (the quiescent luminosity shown by several BH and NS) a distance of $>$ 6.5 kpc is obtained. This, combined with the optical/X-ray luminosity diagram, disfavours the NS case.

5 CONCLUSIONS

We have presented an extensive observational study of the newly discovered X-ray transient MAXI J1807+132 during its 2017 outburst decay. All the observables are consistent with those typically observed in transient LMXBs during outburst. The system displays striking properties such as dramatic changes in the optical spectrum and several re-flares with a periodicity of 6.5 days. We have explored the possible nature of the compact object, and both a NS or a BH accretor are consistent with the observations. While the NS scenario is favoured by the X-ray fitting (see also Shidatsu et al. 2017a) it also requires fine-tuning of other parameters and some of the suggested explanations for the observed phenomenology to be wrong (e.g., re-flares). All considered, we think that MAXI J1807+132 might be very similar to the BH transient GRO J0422+32. Both objects have shown the same transitions between optical absorption and emission lines, as well as re-flares with very similar recurrence times. GRO J0422+32 has an orbital period of 5.1 hr and a M4 donor (Casares et al. 1995; Webb et al. 2000; Gelino & Harrison 2003), a solution very close to that we have found for MAXI J1807+132 if the re-flares are induced by irradiation of the companion star. Both objects have the same quiescent magnitude ($r \sim 21$) but GRO J0422+32 shows donor spectral features in the spectrum, which suggest that its distance of 2.5 kpc could be a lower limit to that of MAXI J1807+132. However, we stress that, in any case, a NS accretor cannot be ruled out and is even favoured by the X-ray modelling. For this to be the case a distance in the range of $\sim$ 1.5–5 kpc would be required. Future observations of the source, either during new outbursts or quiescence, should provide insights on the nature of the compact object and other properties of the source.

ACKNOWLEDGEMENTS

We are grateful to the anonymous referee for useful comments and suggestions that have improved the paper. We acknowledge support by the Spanish MINECO under grant AYA2017-83216-P. Based on observations made with the Gran Telescopio Canarias (GTC), instaled in the Spanish Observatorio del Roque de los Muchachos of the Instituto de Astrofísica de Canarias, in the island of La Palma. The authors are thankful to the GTC team that carried out the ToO observations. We are thankful to Phil Charles, Nathalie Degenaar, Rudy Wijnands, and Tom Maccarone for useful discussion on the nature of the system. The WHT is operated on the island of La Palma by the Isaac Newton Group of Telescopes in the Spanish Observatorio del Roque de los Muchachos of the Instituto de Astrofísica de Canarias. Based on observations made with the Liverpool Telescope operated on the island of La Palma by Liverpool John Moores University in the Spanish Observatorio del Roque de los Muchachos of the Instituto de Astrofísica de Canarias with financial support from the UK Science and Technology Facilities Council. TMD is supported by RYC-2015-18148. MAP's research is funded under the Juan de la Cierva Fellowship Programme (IJCI-2016-30867) from MINECO. MAPT acknowledges support via a Ramón y Cajal Fellowship (RYC-2015-17854). D.M.S. acknowledges support from the ERC under the European Union's Horizon 2020 research and innovation programme (grant agreement No. 715051; Spiders). MOLLY software developed by T. R. Marsh is gratefully acknowledged. The Faulkes Telescope Project is an education partner of LCO. The Faulkes Telescopes are maintained and operated by LCO.

REFERENCES

Armas Padilla M., Degenaar N., Patruno A., Russell D. M., Linares M., Maccarone T. J., Homan J., Wijnands R., 2011, MNRAS, 417, 659
Armas Padilla M., Wijnands R., Degenaar N., 2013, MNRAS, 436, L89
Armas Padilla M., Wijnands R., Altamirano D., Méndez M., Miller J. M., Degenaar N., 2014a, MNRAS, 439, 3908

Armas Padilla M., Wijnands R., Degenaar N., Muñoz-Darias T., Casares J., Fender R. P., 2014b, MNRAS, 444, 902

Armas Padilla M., Ueda Y., Hori T., Shidatsu M., Muñoz-Darias T., 2017a, MNRAS, 467, 290

Armas Padilla M., Wijnands R., Degenaar N., Munoz-Darias T., Jimenez-Ibarra F., Mata Sanchez D., Casares J., Charles P. A., 2017b, The Astronomer's Telegram, 10224

Armas Padilla M., Ponti G., De Marco B., Muñoz-Darias T., Haberl F., 2018, MNRAS, 473, 3789

Arnason R. M., Sivakoff G. R., Heinke C. O., Cohn H. N., Lugger P. M., 2015, ApJ, 807, 52

Arnaud K. A., 1996, in Jacoby G. H., Barnes J., eds, Astronomical Society of the Pacific Conference Series Vol. 101, Astronomical Data Analysis Software and Systems V. p. 17, http://adsabs.harvard.edu/abs/1996ASPC..101...17A

Astropy Collaboration et al., 2013, A&A, 558, A33

Augusteijn T., Kuulkers E., Shaham J., 1993, A&A, 279, L13

Bailyn C. D., Orosz J. A., 1995, ApJ, 440, L73

Belloni T. M., Motta S. E., Muñoz-Darias T., 2011, Bulletin of the Astronomical Society of India, 39, 409

Burke M. J., Gilfanov M., Sunyaev R., 2017, MNRAS, 466, 194

Burrows D. N., et al., 2005, Space Sci. Rev., 120, 165

Campana S., Brivio F., Degenaar N., Mereghetti S., Wijnands R., D'Avanzo P., Israel G. L., Stella L., 2014, MNRAS, 441, 1984

Casares J., Jonker P. G., 2014, Space Sci. Rev., 183, 223

Casares J., Charles P. A., Naylor T., 1992, Nature, 355, 614

Casares J., Marsh T. R., Charles P. A., Martin A. C., Martin E. L., Harlaftis E. T., Pavlenko E. P., Wagner R. M., 1995, MNRAS, 274, 565

Cepa J., et al., 2000, in Iye M., Moorwood A. F., eds, Proc. SPIEVol. 4008, Optical and IR Telescope Instrumentation and Detectors. pp 623–631, doi:10.1117/12.395520, http://adsabs.harvard.edu/abs/2000SPIE.4008..623C

Chambers K. C., et al., 2016, preprint (arXiv:1612.05560)

Charles P. A., Coe M. J., 2006, Optical, ultraviolet and infrared observations of X-ray binaries. pp 215–265, http://adsabs.harvard.edu/abs/2006csxs.book..215C

Chen W., Livio M., Gehrels N., 1993, ApJ, 408, L5

Clemens D. P., 1985, ApJ, 295, 422

Corral-Santana J. M., Casares J., Muñoz-Darias T., Bauer F. E., Martínez-Pais I. G., Russell D. M., 2016, Astronomy & Astrophysics, 587, A61

Cox A. N., 2000, Allen's astrophysical quantities. http://adsabs.harvard.edu/abs/2000asqu.book.....C

Degenaar N., Wijnands R., Miller J. M., 2013, ApJ, 767, L31

Degenaar N., Pinto C., Miller J. M., Wijnands R., Altamirano D., Paerels F., Fabian A. C., Chakrabarty D., 2017, MNRAS, 464, 398

Denisenko D., 2017, The Astronomer's Telegram, 10217

Díaz Trigo M., Parmar A. N., Boirin L., Méndez M., Kaastra J. S., 2006, A&A, 445, 179

Dubus G., Kim R. S. J., Menou K., Szkody P., Bowen D. V., 2001, ApJ, 553, 307

Faulkner J., Flannery B. P., Warner B., 1972, ApJ, 175, L79

Fender R., Muñoz-Darias T., 2016, in , Astrophysical Black Holes. Springer International Publishing, pp 65–100, doi:10.1007/978-3-319-19416-5_3

Foight D. R., Güver T., Özel F., Slane P. O., 2016, ApJ, 826, 66

Galloway D. K., Muno M. P., Hartman J. M., Psaltis D., Chakrabarty D., 2008, ApJS, 179, 360

Gehrels N., et al., 2004, ApJ, 611, 1005

Gelino D. M., Harrison T. E., 2003, ApJ, 599, 1254

Gilmore G., Reid N., 1983, MNRAS, 202, 1025

Hernández Santisteban J. V., Knigge C., Pretorius M. L., Sullivan M., Warner B., 2018, MNRAS, 473, 3241

Jansen F., et al., 2001, A&A, 365, L1

Jiménez-Ibarra F., Muñoz-Darias T., Wang L., Casares J., Sánchez D. M., Steeghs D., Padilla M. A., Charles P. A., 2018, Monthly Notices of the Royal Astronomical Society, 474, 4717

Kalberla P. M. W., Burton W. B., Hartmann D., Arnal E. M., Bajaja E., Morras R., PÃűppel W. G. L., 2005, Astronomy & Astrophysics, 440, 775

Kennea J. A., Evans P. A., Beardmore A. P., Krimm H. A., Romano P., Yamaoka K., Serino M., Negoro H., 2017a, The Astronomer's Telegram, 10215

Kennea J. A., et al., 2017b, The Astronomer's Telegram, 10216

Kennea J. A., et al., 2017c, The Astronomer's Telegram, 10216

Khargharia J., Froning C. S., Robinson E. L., Gelino D. M., 2012, The Astronomical Journal, 145, 21

King A. R., 1993, MNRAS, 260, L5

King A. R., Kolb U., Burderi L., 1996, ApJ, 464, L127

Kubota A., Tanaka Y., Makishima K., Ueda Y., Dotani T., Inoue H., Yamaoka K., 1998, PASJ, 50, 667

Kuulkers E., et al., 2013, A&A, 552, A32

Lasota J.-P., 2001, New Astronomy Reviews, 45, 449

Lin D., Remillard R. A., Homan J., 2007, The Astrophysical Journal, 667, 1073

Makishima K., Maejima Y., Mitsuda K., Bradt H. V., Remillard R. A., Tuohy I. R., Hoshi R., Nakagawa M., 1986, ApJ, 308, 635

Mata Sánchez D., Muñoz-Darias T., Casares J., Corral-Santana J. M., Shahbaz T., 2015, MNRAS, 454, 2199

Menou K., Hameury J.-M., Stehle R., 1999, Monthly Notices of the Royal Astronomical Society, 305, 79

Miller J. M., Raymond J., Fabian A., Steeghs D., Homan J., Reynolds C., van der Klis M., Wijnands R., 2006, Nature, 441, 953

Mineshige S., 1994, ApJ, 431, L99

Mitsuda K., et al., 1984, PASJ, 36, 741

Motta S. E., 2016, Astronomische Nachrichten, 337, 398

Munari U., Zwitter T., 1997, A&A, 318, 269

Muñoz-Darias T., Casares J., Martínez-Pais I. G., 2008, MNRAS, 385, 2205

Muñoz-Darias T., Motta S., Belloni T. M., 2011, MNRAS, 410, 679

Muñoz-Darias T., Fender R. P., Motta S. E., Belloni T. M., 2014, MNRAS, 443, 3270

Muñoz-Darias T., et al., 2016, Nature, 534, 75

Munoz-Darias T., Jimenez-Ibarra F., Mata Sanchez D., Armas Padilla M., Casares J., Charles P. A., 2017, The Astronomer's Telegram, 10221

Negoro H., et al., 2017, The Astronomer's Telegram, 10208

Patruno A., Maitra D., Curran P. A., D'Angelo C., Fridriksson J. K., Russell D. M., Middleton M., Wijnands R., 2016, ApJ, 817, 100

Patterson J., et al., 1998, PASP, 110, 1290

Plant D. S., Fender R. P., Ponti G., Muñoz-Darias T., Coriat M., 2015, A&A, 573, A120

Ponti G., Fender R. P., Begelman M. C., Dunn R. J. H., Neilsen J., Coriat M., 2012, MNRAS, 422, L11

Ramachandran R., Bhattacharya D., 1997, MNRAS, 288, 565

Reis R. C., Fabian A. C., Miller J. M., 2010, MNRAS, 402, 836

Remillard R. A., McClintock J. E., 2006, Annual Review of Astronomy and Astrophysics, 44, 49

Repetto S., Davies M. B., Sigurdsson S., 2012, MNRAS, 425, 2799

Russell D. M., Fender R. P., Hynes R. I., Brocksopp C., Homan J., Jonker P. G., Buxton M. M., 2006, MNRAS, 371, 1334

Russell D. M., Fender R. P., Jonker P. G., 2007, MNRAS, 379, 1108

Shahbaz T., Russell D. M., Zurita C., Casares J., Corral-Santana J. M., Dhillon V. S., Marsh T. R., 2013, MNRAS, 434, 2696

Shidatsu M., et al., 2014, ApJ, 789, 100

Shidatsu M., et al., 2017a, preprint (arXiv:1710.03371)

Shidatsu M., et al., 2017b, The Astronomer's Telegram, 10222

Strüder L., et al., 2001, A&A, 365, L18

Tomsick J. A., Yamaoka K., Corbel S., Kaaret P., Kalemci E., Migliari S., 2009, ApJ, 707, L87

Torres M. A. P., et al., 2008, ApJ, 672, 1079

Turner M. J. L., et al., 2001, A&A, 365, L27

VanderPlas J. T., 2017, preprint (arXiv:1703.09824)

Verner D. A., Ferland G. J., Korista K. T., Yakovlev D. G., 1996, ApJ, 465, 487

Webb N. A., Naylor T., Ioannou Z., Charles P. A., Shahbaz T., 2000, MNRAS, 317, 528

Wijnands R., Degenaar N., Armas Padilla M., Altamirano D., Cavecchi Y., Linares M., Bahramian A., Heinke C. O., 2015, MNRAS, 454, 1371
Wilms J., Allen A., McCray R., 2000, ApJ, 542, 914
Zdziarski A. A., Johnson W. N., Magdziarz P., 1996, MNRAS, 283, 193
Zurita C., et al., 2002, Monthly Notices of the Royal Astronomical Society, 334, 999
Zurita C., et al., 2006, ApJ, 644, 432
Życki P. T., Done C., Smith D. A., 1999, MNRAS, 309, 561
van Dokkum P. G., 2001, PASP, 113, 1420
van der Klis M., 2006, Rapid X-ray Variability. pp 39–112, http://adsabs.harvard.edu/abs/2006csxs.book...39V

APPENDIX A: OPTICAL PHOTOMETRY OF MAXI J1807+132 IN THE 2017 OUTBURST

The photometric data presented in this work are listed in Table A1. They correspond to the SDSS-*g*,-*r*, and -*i* bands. The telescope used in each case is indicated.

This paper has been typeset from a TEX/LATEX file prepared by the author.

Table A1. SDSS-*g*, -*r*, and -*i* photometry of MAXI J1807+132 (LT, LCO, and GTC).

	SDSS-*g* (mag)			SDSS-*r* (mag)		SDSS-*i* (mag)	
Date	LT	LCO	GTC	LT	LCO	LT	LCO
28-03-2017	-	18.76 ± 0.10	18.36 ± 0.01	-	18.54 ± 0.07	-	18.59 ± 0.10
30-03-2017	19.24 ± 0.02	-	19.22 ± 0.02	19.24 ± 0.02	-	19.26 ± 0.02	-
31-03-2017	19.75 ± 0.03	-	-	19.70 ± 0.04	-	19.79 ± 0.04	-
01-04-2017	20.17 ± 0.04	-	-	20.10 ± 0.04	-	20.05 ± 0.06	-
02-04-2017	21.14 ± 0.04	-	-	20.98 ± 0.04	-	20.77 ± 0.04	-
03-04-2017	20.63 ± 0.09	-	-	20.78 ± 0.11	-	20.88 ± 0.17	-
04-04-2017	20.89 ± 0.06	-	-	20.62 ± 0.04	-	20.61 ± 0.06	-
05-04-2017	21.17 ± 0.03	21.09 ± 0.17	-	21.08 ± 0.03	20.69 ± 0.14	20.90 ± 0.04	20.67 ± 0.17
06-04-2017	19.06 ± 0.02	19.14 ± 0.04	19.06 ± 0.02	19.09 ± 0.02	19.22 ± 0.04	19.15 ± 0.01	19.41 ± 0.06
07-04-2017	18.48 ± 0.04	19.86 ± 0.18	18.65 ± 0.05	18.54 ± 0.03	19.74 ± 0.15	18.38 ± 0.02	20.18 ± 0.26
08-04-2017	19.36 ± 0.06	-	-	19.38 ± 0.03	-	19.47 ± 0.03	-
09-04-2017	19.83 ± 0.15	-	-	19.81 ± 0.10	-	19.89 ± 0.08	-
10-04-2017	20.26 ± 0.31	-	-	20.44 ± 0.32	-	20.28 ± 0.24	-
12-04-2017	18.90 ± 0.13	-	-	19.17 ± 0.10	-	19.27 ± 0.08	-
13-04-2017	18.80 ± 0.07	19.35 ± 0.21	-	-	19.66 ± 0.26	18.82 ± 0.04	19.27 ± 0.24
14-04-2017	19.31 ± 0.08	-	-	-	19.52 ± 0.29	19.42 ± 0.07	19.37 ± 0.28
15-04-2017	20.18 ± 0.28	-	-	-	-	19.74 ± 0.12	-
16-04-2017	20.43 ± 0.07	19.89 ± 0.39	-	-	20.41 ± 0.69	20.09 ± 0.08	19.21 ± 0.37
17-04-2017	21.25 ± 0.35	-	-	-	-	-	-
18-04-2017	19.07 ± 0.07	-	-	-	-	18.92 ± 0.08	-
19-04-2017	18.95 ± 0.02	-	-	-	-	18.80 ± 0.02	-
20-04-2017	19.30 ± 0.02	-	-	-	-	-	-
23-04-2017	21.18 ± 0.03	-	-	-	-	-	-
24-04-2017	-	19.75 ± 0.20	-	-	20.70 ± 0.40	-	21.04 ± 0.75
25-04-2017	-	20.49 ± 0.13	-	-	20.10 ± 0.13	-	20.33 ± 0.17
01-05-2017	21.15 ± 0.03	-	-	-	-	-	-
03-05-2017	19.18 ± 0.04	-	-	-	-	-	-
06-05-2017	20.48 ± 0.05	-	-	-	-	-	-
07-05-2017	-	20.35 ± 0.08	-	-	20.66 ± 0.08	-	20.32 ± 0.10
12-05-2017	21.41 ± 0.29	-	-	-	-	-	21.05 ± 0.65
16-05-2017	-	-	-	-	19.10 ± 0.65	-	-
31-05-2017	21.03 ± 0.03	-	-	-	-	-	-
04-06-2017	-	19.49 ± 0.19	-	-	19.46 ± 0.11	-	20.82 ± 0.44
19-06-2017	21.27 ± 0.03	-	-	-	-	-	-
12-07-2017	21.25 ± 0.03	-	-	-	-	-	-
16-07-2017	-	-	21.54 ± 0.08	-	-	-	-
18-08-2017	-	-	21.47 ± 0.04	-	-	-	-